Proceedings World Geothermal Congress 2020+1
Reykjavik, Iceland, April - October 2021

Advanced Self-Healing Polymer-Cement Composites for Geothermal Wellbore Applications up to 300 °C

Phillip K. Koech[2], Carlos A. Fernandez[2*], Kenton A. Rod[2], Gao Dai[2], Nicolas J. Huerta[3], Sarah Burton[4], Quin R. S. Miller[1], and Charles T. Resch[1]

1 Physical and Computational Sciences Directorate, Pacific Northwest National Laboratory, Richland Washington.

2 Energy and Environment Directorate, Pacific Northwest National Laboratory, Richland Washington.

3 National Energy Technology Laboratory, Albany Oregon.

4 Earth and Biological Sciences Directorate, Pacific Northwest National Laboratory, Richland Washington.

* Corresponding author: Carlos.Fernandez@pnnl.gov

Keywords: Polymer-cement, composite, wellbore, self-healing, ductile

ABSTRACT

Polymer-cement composites were formulated using two base cements (cement H and thermal shock resistant cement) and three polymers (a thermoset epoxide-based polymer, Poly(ethylene-co-acrylic acid) zinc salt, and Bisphenol A diglycidyl ether/ Poly(ethylene-co-acrylic acid) and evaluated as potential alternatives to conventional geothermal wellbore cementitious materials. To mimic geothermal conditions, these cement composites were cured at 300 °C and their mechanical properties, including compressive strength, Young modulus, shear bond strength to steel casing, and self-healing and re-adhering (to steel) capability were tested. To test thermal stability the samples were cured at 300 °C for up to 30 days followed by analysis of their mineralogy and chemical composition by X-ray diffraction spectroscopy (XRD), ^{13}C Nuclear Magnetic Resonance spectroscopy (NMR), and total organic carbon (TOC). These tests showed that all polymer composites formulated were thermally stable as supported by the presence of nearly 100% of the original polymer added in samples cured at 300 °C and the presence of all the polymer signals in ^{13}C NMR. Permeability tests performed before and after healing a longitudinal fracture on polymer-cement composites gave lower (post-healing/pre-healing) permeability ratios with respect to base cements which suggests that introduction of polymers result in a composite with self-healing properties. Curing two of the best performing polymer-cement composites for a period of 30 days at 300 °C maintained the self-healing capability. These advanced polymer-cement composites with higher mechanical stability, ductility and self-healing capability are promising alternatives to conventional wellbore cement materials for geothermal and fossil energy applications.

1. INTRODUCTION

Cement is commonly used in geothermal and fossil wellbores in the annulus between the casing and the formation rock to minimize the chances of fluid transport in and out of the casing. However, cement has a tendency to fracture and de-bond from the formation and/or casing[1]. These fractures in wellbore cement in combination with brine and the presence of a high concentration of CO_2 has been shown to compromise the integrity of a wellbore[2]. Furthermore, geothermal wellbores are located in chemically corrosive environments with high temperatures (> 300 °C) which lead to wellbore failure that requires expensive and time-consuming repairs and production interruptions[3]. There is a huge need for self-healing cement materials that will minimize or eradicate wellbore interventions requirements.

Numerous self-healing cementitious materials have been reported, but to the best of our knowledge none can withstand the high temperature and chemically corrosive environments in fossil and geothermal wellbores[4-6]. Continued hydration of residual clinker or the carbonation of dissolved calcium hydroxide results in inherent self-healing of ordinary cement, this process is capable of filling small cracks, (< 60 μm).[5, 7-10] The best self-healing approach for cementitious materials to date involves one-time use capsules containing polymer monomers that are introduced in the cement formulation and distributed in its matrix during curing. Self-healing in this approach is triggered by a crack which breaks the capsules thus releasing the monomer that subsequently initiates a polymerization reaction filling the crack. This process has a rapid healing mechanism, but the composites are limited to single repair events due to the irreversible healing reactions.[11-13] Other self-healing cements consisting of inorganic components with delayed ability crystalize have been reported, but often require the presence of fluids such as water, CO_2, or oil to form adequate chemical materials to reseal the cracks.[5, 7, 14-16] Additionally, the reaction rates of these inorganic materials are slow (weeks to months) rendering this process ineffective. Bacterially-induced calcium carbonate precipitation has been proposed as an environmentally friendly self-healing technique for cementitious materials.[17] Like the inorganic self-healing cements, these precipitation reactions take up to 5 weeks to generate enough material to heal small cracks (< 10 microns).[18] This slow healing process is a major drawback because the rate of crack formation and propagation in cementitious cement can be significantly higher than healing material production, leading to crack maturation to aperture compromising self-healing ability. Furthermore, high temperatures in geothermal environments will not be suitable for survival of bacteria. In our recent study we reported the development of self-healing polymer-cement composite with potential application in geothermal and fossil energy.[3, 19] The difference between this polymer-cement composite and all the self-healing cement materials discussed above is the self-healing mechanism which is achieved through addition of small concentration (up to 10wt%) of thermally stable self-healing polymers to the cement without the need of a carrier.[20-24] In this polymer-cement composite multiple self-healing events occur due to reversible and dynamic polymer-polymer and polymer-cement bonding.[3, 19] Furthermore, this novel self-healing cement composite materials have been demonstrated to be stable at geothermal temperatures[25-28].

Encourage by this seminal results, polymer-cement composites derived from three self-healing polymers and two wellbore cement materials were formulated and their thermal stability was tested by curing at elevated temperature (300 °C) for up to 30 days. The material mechanical properties such as bond strength, compressive strength, Young's modulus, and permeability were tested. To evaluate the stability of these polymer-cement composites in typical geothermal environments, total organic carbon (TOC), nuclear magnetic resonance spectroscopy (NMR), and X-ray diffraction spectroscopy (XRD) were performed. In addition, compressive strength and self-healing capability was evaluated on these cement composites after exposure to different thermal and chemical stresses. The results show that these self-healing cements represent a major advance in wellbore cementing for cost-effective and environmentally responsible geothermal and fossil energy production.

2. METHODS

2.1 Preparation of Polymer-Cement Composites

Polymer-cement composite used in this study were made by combining two different wellbore cements with three polymer formulations. The two wellbore cements used were: 1) class H Portland cement (class H; Lafarge) was a 70:30 mixture of class H Portland cement and silica flour (US silica), and 2) Thermal Shock Resistant Cement (TSRC) developed by Pyatina and Sugama [29], which has a mixture of 53.5 wt.% calcium aluminate, 35.5 wt.% class F fly ash, 6 wt.% carbon microfiber, and 5 wt.% sodium metasilicate, and obtained courtesy of Brookhaven National Laboratory. The polymers used included Thioplast EPS 25 (EPS 25) (640 g/1 equivalent epoxide) supplied by Akzo Nobel, and 4-dimethylaminopyridine (DMAP), poly(ethylene glycol) diglycidyl ether (PEO) (250 g/1 equivalent epoxide), pentaerythritol tetrakis(3-mercaptopropionate) (4SH), Poly(ethylene-co-acrylic acid) zinc salt powder (Zn-salt), Bisphenol A diglycidyl ether (BPA) purchased from Sigma-Aldrich, N,N-Dimethylethylenediamine (NND), Ethylenediamine (ED) were purchased from Sigma-Aldrich. All materials were used as received. The composite formulations are listed in Table 1 including the percentage of each polymer precursor and wt.% of monomers.

Table 1: All composites resulting from the cements and polymer systems explored in this study.

Composite	Cement	Polymer (in dry mixture)
Class H Base	Class H:silica flour	N/A
Class H + Zn Salt	Class H:silica flour	15 wt% Zn Salt
Class H + Zn Salt BPA	Class H:silica flour	10 wt% Zn Salt + 5% (BPA, N, N ED, ED)
Class H + EPS 25	Class H:silica flour	10 wt% (EPS 25, PEO, 4SH; mass ratio 1:1:0.68)
TSRC Base	TSRC	N/A
TSRC + Zn Salt	TSRC	15 wt% Zn Salt
TSRC + Zn Salt BPA	TSRC	10 wt% Zn Salt + 5% BPA (BPA, PEO, NND, ED; mass ratio 1: 1: 0.32: 0.038)
TSRC + EPS25	TSRC	10 wt% (EPS 25, 4SH, PEO; mass ratio 1:1:0.68)

The cement slurries were prepared by mixing the dry powder materials using a Caframo overhead mixer with a 4 x 2 -impeller. Mixing continued for 10 minutes, after which any required polymer that is liquid at room temperature was added to the cement slurry. All of the slurries were then mixed for an additional 5 minutes to ensure the composites were homogeneous.

2.2 Pipe Shear Bond Strength (SBS) Tests

To evaluate the bond strength of cement composites to steel adhesion and re-adhesion test were conducted in triplicate using a confined method similar to previously performed tests [30-31]. The test involved two thick walled, 316 stainless steel pipes aligned with their sides parallel to each other, by use of an end cap jig. Pipe dimensions were: 1) inner pipe of 12.7 mm diameter and 50.8 mm long and outer (confining) pipe of 38.1 mm diameter x 38.1 mm. Cement composite slurries were poured into the annulus between the inner and outer pipes after pouring the cement in the annulus was tamped well to free any trapped air. Samples were cured at room temperature for 24h in 100% relative humidity (RH), followed by 24h at 85 °C and 100% RH, and finally five days at 200 °C in a Parr reactor at 100% RH. Once the curing process was completed, the samples were carefully removed from the bottom end cap. Shear bond strength tests were performed using a test frame model MTS 50Kip in conjunction with Bluehill by Instron controls and data acquisition software. Sample was placed inside of a test jig with the inner pipe protrusion up. Force was applied at a rate of 1,800 lb/min, with the maximum load defined as the force required to cause the inner pipe to initially slip. Once the test was completed the sample was inverted and the inner steel pipe compressed back to its original position for the second "after heal" test. The samples were reacted a second time at 300 °C in a Parr reactor at 100% RH after which the adhesive bond strength was tested again. The shear bond strength is calculated following API Specifications 10A, using equation 1:

$$SBS = \frac{P}{A} \tag{1}$$

where SBS = shear bond strength (psi); P = maximum load (lbf); A = area of bonding surface (in^2)

2.3 Compressive Strength Analysis

Cement monoliths with an average length of 8.2 cm (±0.5) and diameter of 2.5 cm (±0.03) were tested for compressive strength using standard methods (ASTM C39/C39M-15a). Before conducting the tests, the monolith ends were cut, using a rock saw, perpendicular to the length to provide a flat surface minimizing point loading during tests. Tests were performed using an MTS model 312.31 servohydraulic frame with a 55-kip actuator and load cell. The loading rate was 1800 psi/min and cardboard shims were placed between the plate and sample on both ends to absorb potential point loading from sample defects that could increase the risk of test failure.

2.4 Young Modulus Analysis

To calculate Young's Modulus, stress and strain were measured during mechanical testing of the specimens. Tests were performed using an MTS 312.21 servohydraulic universal test frame controlled by Instron Bluehill 2 software. Samples were spatter painted before testing, creating dark contrasting speckles on light colored surface. Stress-strain data was collected using video capture of compression tests with the prepared samples, measuring movements of speckles relative to each other. Load and displacement data are collected during testing and used to calculate stress and strain in the sample throughout the test. The stress-strain curve generated was used to determine the Young's modulus. The elastic modulus of the sample is the ratio of stress to strain in the sample which was calculated by determining the slope of the curve in the elastic region of the test.

2.5 Magic Angle spinning Nuclear Magnetic Resonance (MAS-NMR)

^{13}C NMR was used to analyze the carbon functional groups present in cured cement samples. The ^{13}C NMR spectra were collected using 300 MHz Varian Inova console. The probe used was a 5 mm HX Chemmagnetics style probe with a ceramic housing and the samples were contained in zirconia rotors with boron nitride spacers. Samples were spun at 5 kHz or 8 kHz. The variable amplitude cross polarization (vacp) pulse sequence experiments were run with a 4 μs 90-degree pulse, 2 ms contact cross polarization pulse, and 62 kHz proton decoupling for 10 ms.

2.6 Total Organic Carbon (TOC)

The powder cement samples were analyzed for total carbon (TC) and inorganic carbon (IC) with a Shimadzu Total Organic Carbon Analyzer, Model TOC-L CSH/CSN, outfitted with a Solid Sample Module, Model SSM-5000A (Shimadzu Scientific Instruments, Inc., Columbia, MD 21046). Samples and standards were weighed into ceramic sample boats that were pre-cleaned with 2N hydrochloric acid (diluted from Fisher Scientific catalog# A144C-212, lot# 043414), rinsed with deionized water, dried, and then fired at 900 °C in a muffle furnace for 30 minutes. The TC was determined by combustion at 900 °C. The IC was determined by adding 85% phosphoric acid (Fisher Scientific catalog# A260-500, lot# 076856) to the sample at 200 °C. A non-dispersive infrared (NDIR) gas analyzer was used to detect the resultant carbon dioxide gas. The total organic carbon (TOC) was determined by difference, TOC = TC-IC. Dextrose (D-glucose) solid was used for the TC calibration ($C_6H_{12}O_6$, 40.0% C, Fisher Scientific catalog# D16-500, lot # 170457). Sodium bicarbonate was used for the IC calibration ($NaHCO_3$, 14.3% C, Fisher Scientific catalog# S233-500, lot# 172497).

2.7 X-Ray Diffraction (XRD)

Powder X-ray diffraction (XRD) analysis of the cement and polymer-cement composites was conducted with a Bruker D8 Discover (Bruker AXS Inc., Madison, WI), equipped with a rotating Cu anode (Kα λ = 1.5418 Å), capable of producing an intensely focused 0.5 mm beam. Samples (~10 mg) were lightly pressed into a vertically-oriented stainless-steel sample holder, mounted in the XRD on a custom-built programmable XYZ stage, and positioned using a laser-video alignment system. A Vantec 500 area detector system positioned at 22 and 40 °2θ with a measured sample-detector distance of 15 cm was used to capture diffraction images with a range of 6.0-54.2 °2θ. Collection of individual XRD tracings required 200 seconds with power settings of 50 kV and 25 mA and a vertical sample oscillation of 1.0 mm. Initially, images were processed with Bruker-AXS GADDS software before importing into MDI JADE XRD software to obtain peak positions and intensities and identify minerals using the International Centre for Diffraction Data (ICDD) powder diffraction file (PDF) database. Reported phases are identified below with their ICDD PDF# specified in parentheses. More information about the XRD methods, including sample loading, data acquisition, and data analysis can be found in Miller et al. [32-33]

2.8 Fractured Sample Generation and Permeability Measurements

Cylindrical cement samples with length between 2.9 cm and 9.7 cm and diameter of 2.5 cm were tested for fracture permeability using tap water. Samples cured, for either 5 days or 30 days, were cut to length with a rock saw. The samples were then fractured along their length by using a modified version of the Brazilian test[34], which is used to fail a sample in tension. To generate a fracture, the sample was placed horizontally into a core splitter (Pothier Manual Core Splitter) so that the lower platen and upper blade would apply force along the length of the sample. The splitter's upper blade was then screwed down via the hand wheel so that the sample was secured between blade and platen. A rubber mallet was then used to apply force onto the rod cap, which transmitted this force onto the sample and caused a tensile failure. The resulting fractured sample was then cleaned of any loose debris. The fractured cores were reassembled using either Polyolefin plastic heat-shrink tubing (McMaster-Carr).

Fracture permeability was tested using a variation of the constant head method[35-36] where constant head was maintained by maintaining the reservoir at a constant fluid level (i.e., hydraulic head) and effluent mass was measured at periodic intervals. A constant density of water (1 g m^{-3}) was used to convert the measured mass to volume. Reynolds equation (Equation 1) for flow through fractured media with Darcy's law (Equation 3), with cross sectional area being the aperture times width (Wb) of the fracture, was arranged for calculation of permeability (Equation 4)[37]:

$$Q = -\frac{Wb^3}{12v}\left(\frac{P_0 - P_i}{l}\right) \quad (2)$$

$$Q = -\frac{k_i W b}{v}\left(\frac{P_0 - P_i}{l}\right) \quad (3)$$

$$k_i = \frac{b^2}{12} \quad (4)$$

where Q = Volumetric flow rate ($cm^3\ s^{-1}$); W = effective fracture width (cm); b = fracture hydraulic aperture (cm); v = kinematic viscosity of water ($cm^2\ s^{-1}$); P0 – Pi = Pressure change across fracture length (cm water at 4 °C); l = length of sample (cm); ki = permeability (cm^2).

For the calculations the effective fracture width (W) was estimated to be the diameter of the monolith.

After initial (1st) test was performed the samples were reacted again at 200 °C and 100% RH for five days. A 2nd test for permeability was performed after this second, "heal", reaction.

3. RESULTS AND DISCUSSION

3.1 Shear Bond Strength (SBS)

Confined pipe-shear tests were performed in order to evaluate initial SBS/adhesion and re-adhesion of the polymer cement composite to steel (Figure 1). These tests performed on pure cements and cements polymer composites showed that all class-H based formulations have a bond strength greater than 1000 psi for initial tests and all TSRC derived cement have bond strength greater less 1000 psi for initial tests (Figure 1). Cement cured at the interface with steel have been shown to form carbonate species such as $FeCO_3$ and $CaCO_3$ [38] which would co-precipitate and form a strong O-Fe bond between casing and cement resulting in the high SBS as seen with class H, and class H-polymer composites (Figure 1). The initial SBS for pure TSRC cement is significantly lower than those of TSRC Zn salt and TSRC Zn salt BPA and could be attributed to coordination bonding between the carboxylate of the Zn salt and iron in the casing as well as the high adhesive strength BPA has to steel. The latter is due to interactions between the hydroxyl group and the aromatic rings of the epoxy adhesive and the Fe surface owing to charge transfer from the *d* orbital of Fe to the *p* orbital of the O atom of the hydroxyl group and the π orbitals of the aromatic rings.[19]

SBS values after re-adhesion of the confined cement composites to steel show that these materials have ability to re-adhere to steel, but the recovery of the bond strength is low (Figure 1). The highest ratio of recovery was TSRC Zn-salt BPA (0.79), followed by class H EPS25 (0.50), and TSRC Zn salt (0.38); (Figure 1). In the case of EPS25-class H composites the recovery could be attributed to the re-formation of covalent bonds and hydrogen bonding between the polymer and iron of the casing.[3, 19, 39] In the case of Zn salt BPA, coordination bonds between the carboxylate of the Zn salt and iron of the casing are predicted though BPA has been reported to have strong adhesive interactions with steel surfaces.[3, 19] The authors postulate that after debonding occurs between cement and polymer at these curing temperatures, high mobility polymer migrates to the cement-steel interface and form bonds with steel. The strength of these bonding interactions seems to be similar or stronger than the base cement-casing bonds resulting in similar or higher SBS recovery values. Furthermore, we recently demonstrated that curing times play a critical role in the development of composite-steel bonding strength showing higher strengths when the composite steel samples were cured for 10-15 days as compared to 5 days.[40]

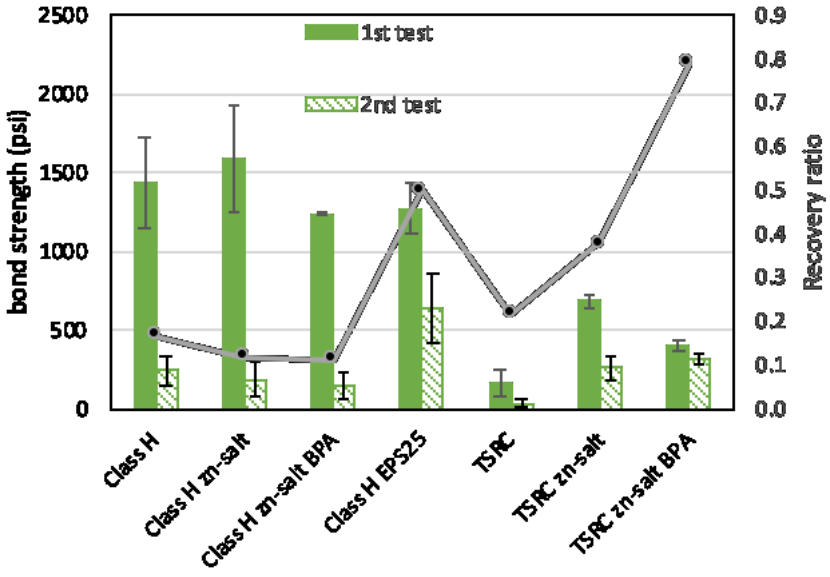

Figure 1. Shear bond strength (SBS) cement-stainless steel: a) of cement and cement composite samples cured for 5 days at 300°C, followed by a 5-day healing event at 300°C and a second shear bond test; b) results of the same tests depicted as ratio of recovery with the ratio being 2nd test: 1st test (bars). c) Recovery ratio is shown in a line represent the same results in the bar in a different way.

3.2 Compressive Strength

Compressive strength is one of the most important mechanical property in wellbore cements. This has led to development of many standard compressive strength test methods. In this study we use an ASTM measurement protocol that is described in the methods section. Compressive strength data was collected for each composite cement material as shown in Figure 2. This data shows that both base cements Class H and TSRC have higher compressive strength than the corresponding polymer-cement composite materials. This reduction in compressive strength is attributed to presence of polymers in the cement matrix which cause possible incomplete hydration of cement[3]. The Class H base cement samples have a higher compressive strength, which is associated to heat-induced early hydration[41]. Similarly, TSRC base cements have higher compressive strength than its polymer-cements. Fly ash in TSRC have been shown to increase compressive strength due to C-S-H gels formed through pozzolanic reactions,[42] however the presence of polymer retards/delays the activity of the fly ash. EPS 25-modified cements show slightly lower compressive strength values than the Zn salt BPA system. The compressive strength values of polymer-cement composites are lower than those of the polymer-free base cements after 24 hours, but these values are mostly well above 1000 psi minimum required for geothermal wellbores application. The only exception to this requirement is the TSRC EPS 25 composite which has slightly lower than 1000 psi compressive strength.

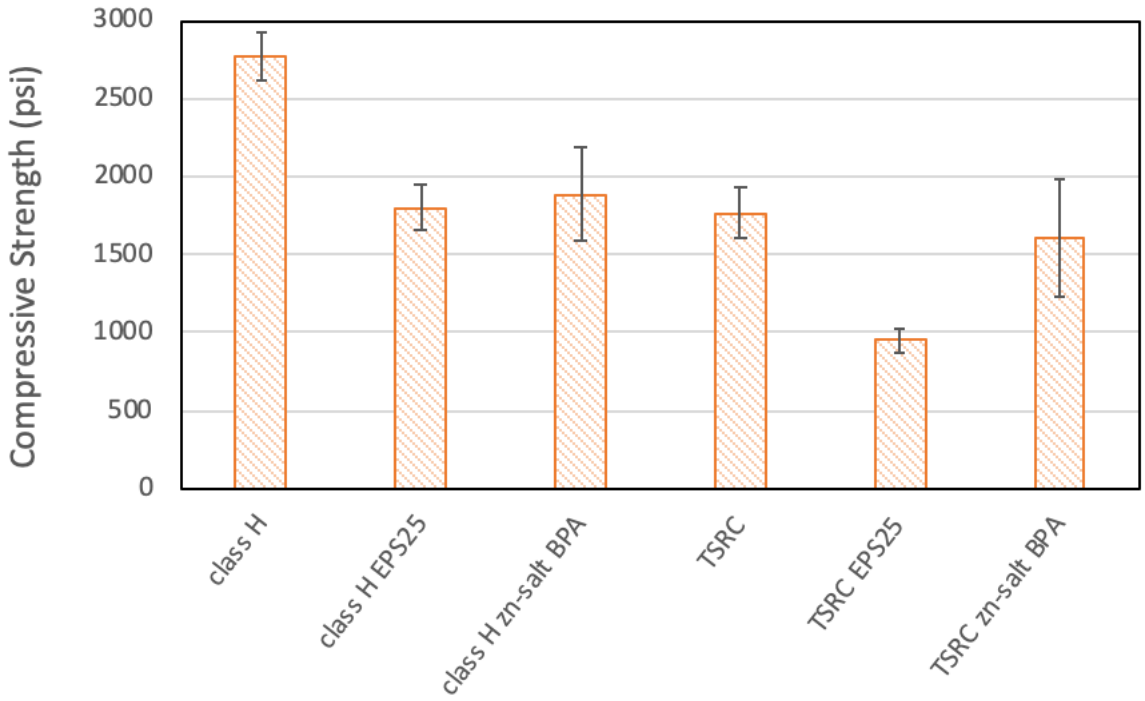

Figure 2. Compressive strength of cement and cement composite materials after curing at 300 °C for 24 hours.

3.3 Young's Modulus

Young's modulus of a material is defined as the ratio of stress /strain and is a measure of how the material responds to uniaxial (tensile or compressive) stress. In order to evaluate the ductility of polymer cement composites compared to base cement materials Young's Modulus tests were performed. Geothermal cement materials should be ductile and not brittle to reduce/minimize fracture propagation under extreme temperatures and pressures in sub-surface environments. The Young's modulus data obtained for Class H, TSRC, and the corresponding polymer-cement composites are shown in Figure 3. Figure 3 data shows that class H cement has the highest Young's modulus values and addition of polymers (Zn salt, Zn salt BPA, and EPS 25) to this cement consistently reduces the Young's modulus compared to the unmodified cement. It is important to mention that Class H-EPS 25 composite showed though statistically similar values of Young's modulus to base cement H. Similarly, addition of Zn salt and BPA Zn salt polymers to the TSRC cement also results in a decrease in Young's Modulus value compared to the unmodified TSRC. This demonstrate that polymer-cement composites are more ductile materials than their unmodified (base) cements. These more ductile materials are suitable for wellbore applications since, in principle they are more resistant to mechanical and thermal stresses.

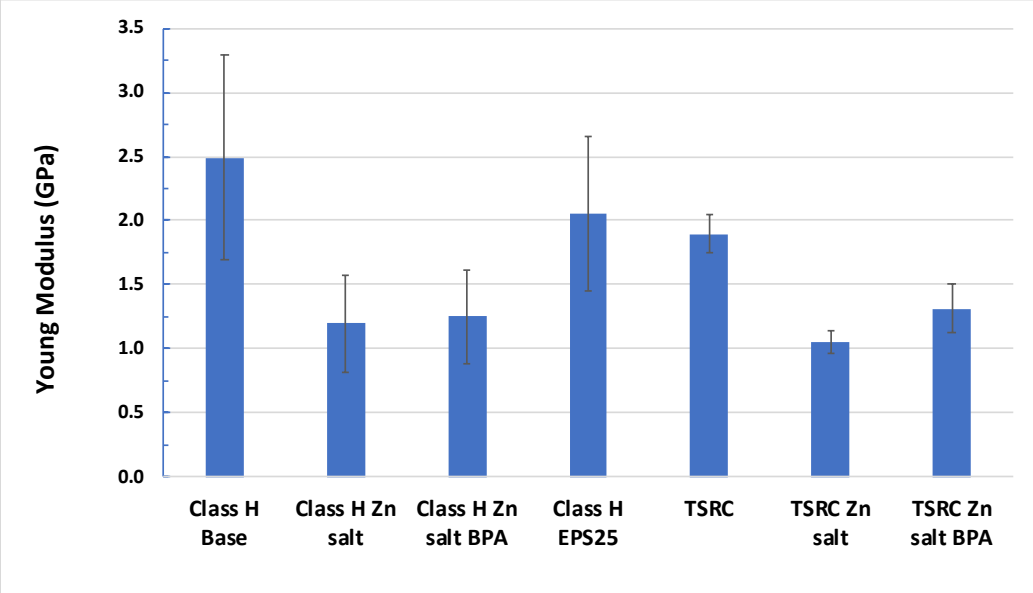

Figure 3. Young's Modulus of cement and cement composite samples after curing at 300°C for five days.

3.4 Total Organic Carbon (TOC)

To evaluate the stability of the polymer in the cement composite matrix at high temperature (300 °C) and pressure similar to wellbore conditions, total organic content (TOC) analysis was performed for cylindrical cement samples cured for 10 days at 300 °C in an unconfined environment (directly exposed to water and water vapors), i.e., worse-case scenario. Table 2 shows a small amount <0.3% TOC present in Class H base unmodified cement. On the other hand, Class H + Zn salt composites had a TOC average value of 9.0wt%. Considering the mass of polymer added originally and normalizing the mass of carbon and corresponding polymer to the final mass of cured cement (having a 17 wt% water loss during cement curing) the value of TOC should have been similar or greater than 6wt%. The high (9.0 wt%) value measured can be attributed to the inhomogeneity of the sample or sampling errors. However, these results indicate that Class H + Zn salt polymer composites is stable at 300 °C for 10 days (Table 2). Class H + Zn salt BPA had a TOC of 7.5 wt% after curing at 300 °C for 30 days. This is still within the expected organic content greater than 6 wt% like for Class H + Zn salt composite.

The TSRC control (base, unmodified cement) contains 5.3 wt% of TOC resulting from the carbon fiber in the formulation Table 2. The modified TRSC Zn salt BPA polymer composite has TOC of 13.3 wt%. If all the polymer is present in the composite and, once again normalizing to mass loss due to water evaporation (6 wt% for these formulations) the value of TOC for the polymer calculated should be 12.6 wt% considering 7.2wt% of carbon fiber. Then, a TOC value of 13.3 wt% in the cement composite cured for 10 days represent ~ 100% of the polymer originally added polymer.

In summary, TOC data shows that the polymers composites of both Class H and TSRC are stable at 300 °C. However, 10 days does not compare to the 30 years of average lifetime of a geothermal wellbore, these results indicate that, these unconfined polymer-cement composite materials are stable under geothermal conditions. More studies need to be performed on these polymer-cement under real, confined, wellbore environments for reliable long-term stability in wellbores.

Table 2: TOC results of composite materials after curing at 300 °C

Composite	Curing Time (Days)	Average TC weight %	Average TIC %	Average TOC %
Class H Base	10	< 0.3	<0.3	< 0.3
Class H + Zn Salt	10	9.0	0.7	8.3
Class H + Zn Salt BPA	10	7.5	< 0.6	7.5
TSRC Base	10	5.3	< 0.8	5.3
TSRC + Zn Salt BPA	10	13.3	< 0.3	13.3

3.5 Magic Angle Spin Nuclear Magnetic Resonance (MAS NMR) Spectroscopy

To confirm the presence of the organic polymers in the cement composites solid state ^{13}C MAS NMR spectroscopy performed. Figure 4 shows three ^{13}C NMR spectra, 4a corresponds to unmodified Class H cement, 4b is the ^{13}C NMR spectrum of Zn Salt/BPA polymer, and 4c show the ^{13}C NMR spectrum of the Class H polymer-cement cured at 300 °C for 10 days. The ^{13}C NMR spectrum 4a shows that the original class H base cement has no organic carbon. The Zn Salt BPA polymer formulation shows ^{13}C NMR signals consistent with the polymer composition that is methylene and methane at 31 ppm, ether methylene at 60 ppm, aromatic groups signal between 120-140 ppm, and the carboxylate and carboxylic acid showing up at ~180 ppm. The 300 °C cured Zn salt BPA polymer-cement H composites exhibit the same ^{13}C NMR characteristic as the original polymer formulation with broadening of the signals which may indicate interaction of the polymer with the cement matrix. These results are not quantitative but confirm the presence of the polymer in its original state at 300 °C, which is critical to demonstrate thermal and chemical stability of the polymer in the cement matrix.

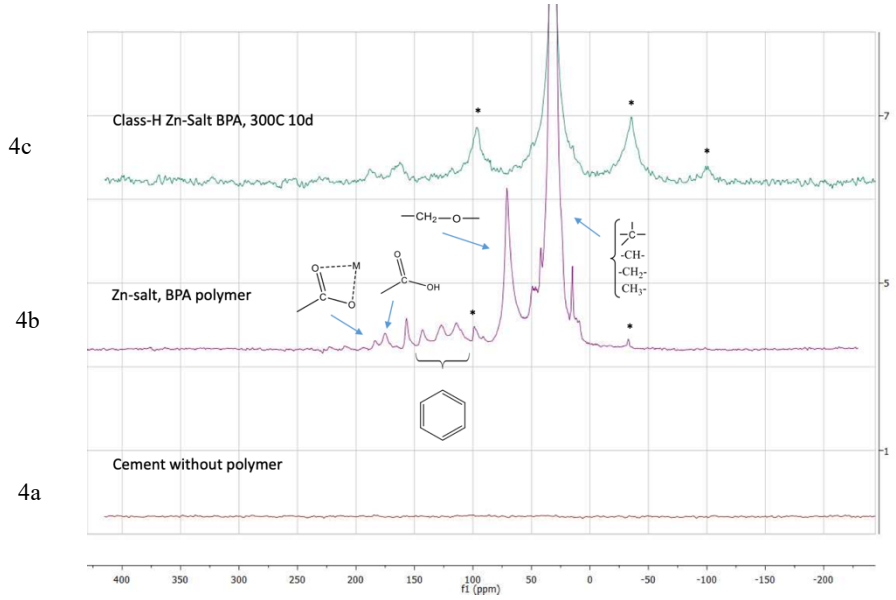

Figure 4. ^{13}C cross-polarization (CP) data collected for base cement H (bottom), Zn salt / BPA polymer (middle), and Zn salt BPA polymer-cement H composite (top). For the pure polymer sample the different carbon species from the polymer are easily identified. When the polymer is cured with cement H at 300 °C for 10 days forming the composite material, the chain carbons and carbonyl carbons are still visible. The CP data indicates that these species must be the most rigid/easiest to cross polarize.

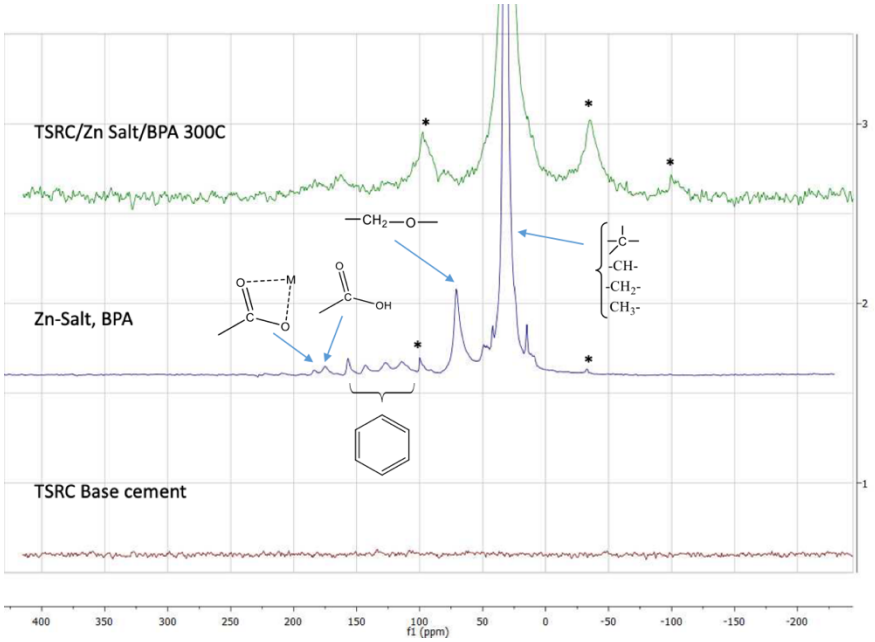

Figure 5. ^{13}C cross-polarization (CP) data collected for base TSRC (bottom), Zn salt / BPA polymer (middle), and Zn salt BPA polymer-TSRC composite (top). When the polymer is cured with cement H at 300 °C for 10 days forming the composite material, the chain carbons and carbonyl carbons are still visible.

Figure 5 shows MAS NMR ^{13}C NMR spectra for TSRC base cement, Zn salt BPA polymer formulation and the corresponding TSRC-polymer cement composite. As discussed previously Zn salt BPA polymer has signals consistent with the polymer. ^{13}C NMR spectrum of TSRC base cement show no ^{13}C NMR signals confirming the absence of carbon in the pure cement. ^{13}C NMR spectrum of TSRC Zn salt BPA polymer-cement composite shows that all the Zn salt BPA polymer signals are present in the sample when cured at 300 °C for 10 days.

3.6 X-Ray Diffraction

3.6.1 Composites based on class H cement

The XRD scans for the Class H cements showed strong similarity of the base cement with the corresponding polymer-based composite, indicating virtually identical mineralogical composition (Figure 6). All four samples were predominantly composed of xonotlite [23-0125, $Ca_6Si_6O_{17}(OH)_2$]. The base cement and the EPS 25-modified cement were nearly monomineralic, with all reflections present assignable to xonotlite. Only the Zn- and Zn+BPA-modified cements displayed identifiable peaks for minor silica and carbonate phases. For those two samples, minor quartz (33-1161, SiO_2) and coesite (014-0654, SiO_2) peaks were resolvable at 39.6 and 39.4 °2θ, respectively, with a higher-intensity quartz reflection also visible at 26.6 °2θ. The presence of calcite (66-0867, $CaCO_3$) in the Zn- and Zn+BPA-modified cements was determined based on the primary calcite peak at 29.4 °2θ (Figure 6). Another possible calcium silicate mineral, tobermorite [i.e. 19-1364, $Ca_5(OH)_2Si_6O_{16}{\cdot}4H_2O$], was not definitively observed to be present in the samples. Although tobermorite's primary peak at 29.0 °2θ could potentially have been present and overlapping with primary xonotlite peak at the same position, the (002) and (222) tobermorite reflections were not present at 7.8 °2θ (not shown) or 30.0 °2θ, respectively.

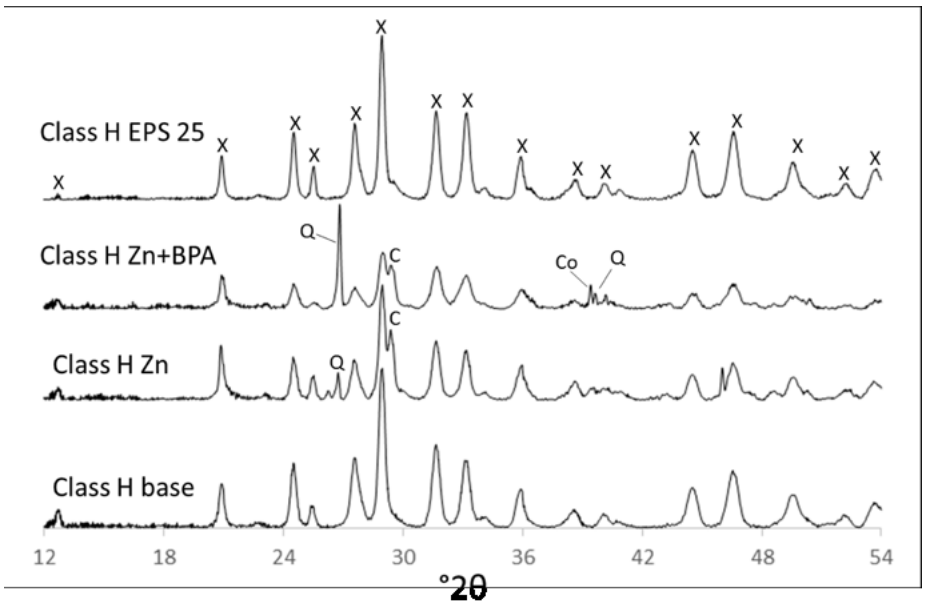

Figure 6. Collected XRD patterns of base cement and polymer-cement composites, offset for clarity, with labeled peaks indicating assigned minerals. See text for ICDD powder diffraction file numbers and further discussion of phase assignments. Mineral abbreviations: Q=quartz; X=xonotlite; C=calcite; Co=coesite.

3.6.2 Composites based on TSRC

Based on the near complete overlap of the collected diffractograms, the mineralogical compositions of all four TSRC cement samples were virtually indistinguishable (Figure 7). Dmisteinbergite (CaAl2Si2O8) was the primary phase present in all three TSRC samples. Dmisteinbergite reflections, collectively assignable to PDF#'s 51-0064, 04-011-5220, and 31-0248, dominated the cement XRD patterns, with the most intense peaks visible at 23.5, 20.2, 31.7, and 35.3 °2θ. Another clearly identifiable phase present was boehmite [5-0190, AlO(OH)], with characteristic peaks at 14.5, 28.3, and 38.4 °2θ. Sodalite (37-0476, $Na_4Al_4Si_3O_{12}Cl$) was present in the samples based on distinguishable peaks at 14.1 and 43.3 °2θ (Figure 7). A micaceous component, likely margarite [018-0276, $CaAl_2(Si_2Al_2)O_{10}(OH)_2$], was identified by a peak at 27.8 °2θ. The samples also contained analcime [19-1180, $Na(Si_2Al)O_6{\cdot}H_2O$], based on peaks located at 25.7 °2θ. Other poorly-developed minor peaks in the diffractograms, including 19.2 and 32.8 °2θ, were likely indicative of gismondine (38-0382, $CaAl_2Si_2O_8{\cdot}4H_2O$).

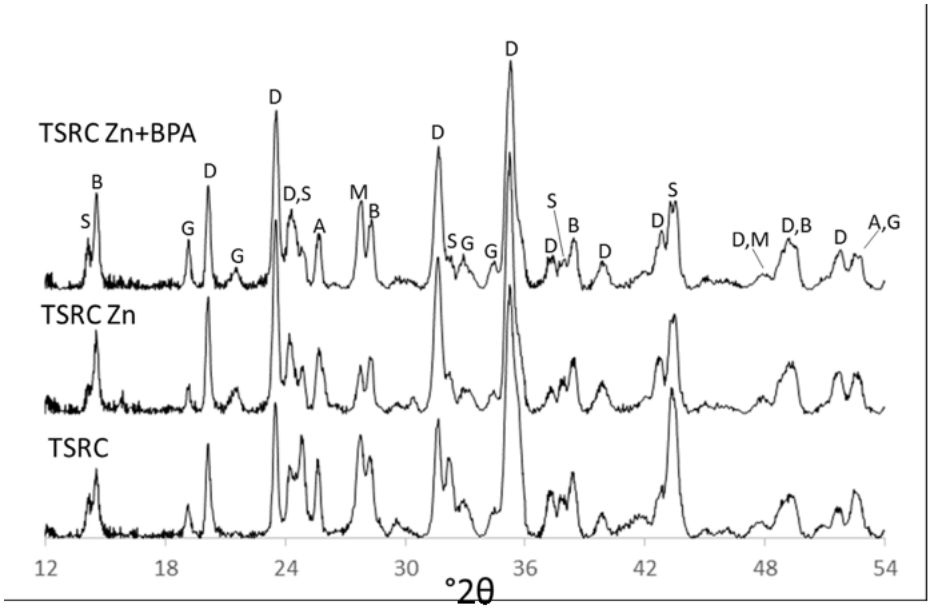

Figure 7. Collected XRD patterns of TSRC and polymer-TSRC composites, offset for clarity, with labeled peaks indicating assigned minerals. See text for ICDD powder diffraction file numbers and further discussion of phase assignments. Mineral abbreviations: A=analcime; S=sodalite; B=boehmite; G=gismondine; D=dmisteinbergite, M=mica.

3.7 Permeability Studies

To evaluate the ability of a cement composite to seal a longitudinal fracture, saturated permeability tests were conducted, with repeats, before and after a five day "heal" reaction. These permeability tests were performed by triplicate on samples initially cured at 300 °C for five days and on samples initially cured 30 days (Figure 8 and 9, respectively). The objective of curing samples for different times was to evaluate if the self-healing capability of the polymer-cement composites is maintained independently of the time at which they were thermally exposed. The samples cured at 300 °C for 5 days were tested for permeability after a fracture was induced (before healing) and after a healing event (post-healing). The permeability values were used to compute a permeability constant K, which is a ratio of 2nd (post-healing) to 1st (before healing) permeability values. As seen in Figure 7, the permeability ratio for the cement composites containing zinc salt decrease post-healing relative to the base cement with exception of TSRC + Zn Salt composite. Any reduction in permeability on the Class H cement could be attributed to calcite formation in the relativity narrow fractures. Both class H Zn Salt and TSRC Zn Salt BPA samples showed over 50% reduction in permeability which is indicative of the self-healing of the composites. Surprisingly, TSRC + Zn Salt composite was the only composite that did not show a reduction but rather an increase in permeability post-healing. These authors don't have an explanation for this result though could be associated to the presence of carbon fibers in TSRC that reduce Zn salt polymer-TSRC bonding interactions/polymer mobility since the composite equivalent, class H Zn salt, showed self-healing capability. Nevertheless, we selected Class H + Zn Salt BPA and TSRC + Zn Salt BPA cement composites to cure for 30 days at 300 °C followed by testing permeability after a shear fracture. The results are shown in Figure 8. The 30-day cured samples permeability data show that both cements composites have a reduction of 60% in permeability post-healing relative to the base cements. These results demonstrate that introducing 10-15wt% polymers to cement results in self-healing composite materials (Figure 8 and 9) which is has been reported to be due to reversible and dynamic polymer-polymer and polymer-cement bonding interactions. [3, 19].

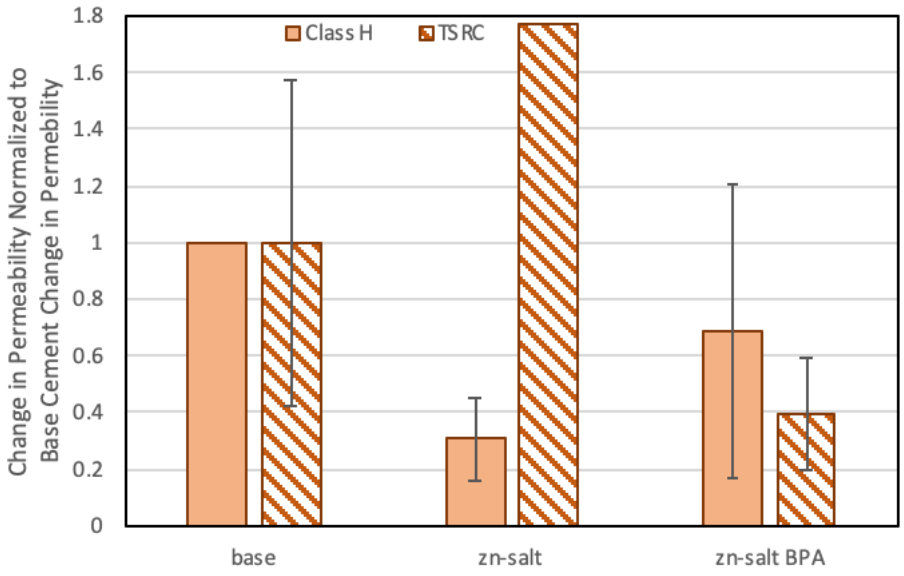

Figure 8. Permeability data of composite materials. Ratio of permeability (K) change normalized to base cement ratio of permeability change (ratio = K after heal: K before heal) of 1" diameter by 3" long samples cured at 300 °C.

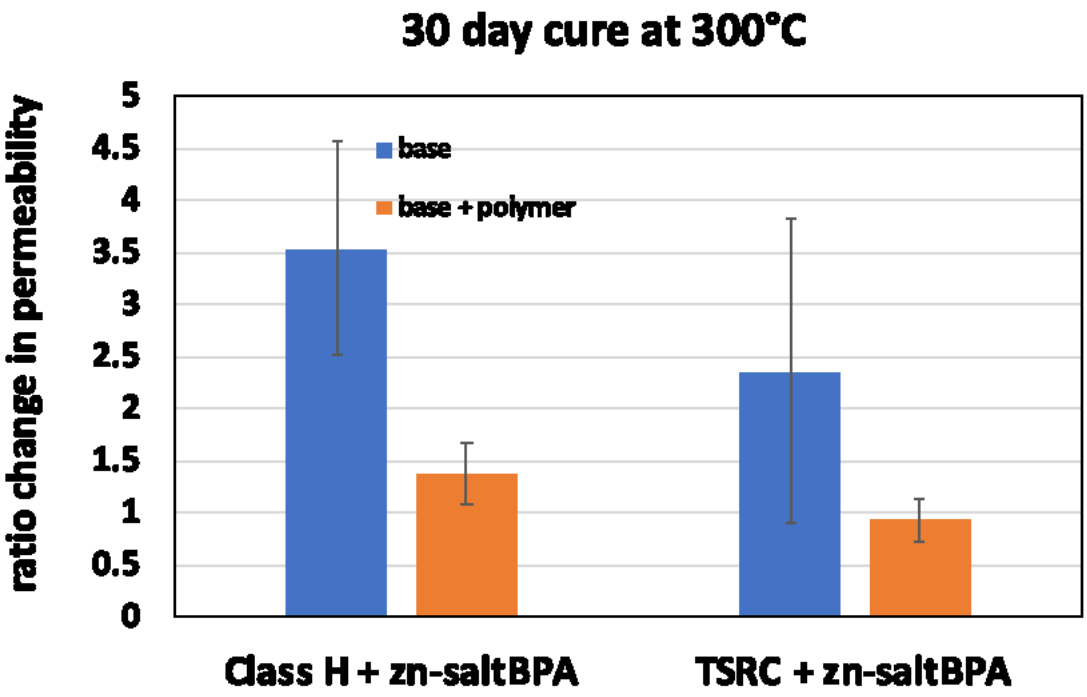

Figure 9. Permeability data of Class H base (in blue), Class H + Zn Salt BPA (in orange), TSRC base (in blue), and TSRC + Zn Salt BPA (in orange) cured at 300 °C for 30 days. Ratio of permeability (K) normalized to each base cement ratio of permeability change (ratio = K after heal: K before heal) of 1" diameter by 3in-long samples.

4. CONCLUSIONS

In this study we formulated polymer-cement composite materials in order to evaluate their potential application in high temperature and pressure geothermal wellbores environments. These polymer cement composites were synthesized using two base cement materials with three different polymer additives. The cement composites were cured at 300 °C for both 5 and 30 days to evaluate their stability as well as the self-healing ability at elevated temperatures such as those found in EGS. Polymer cement composites were found to be significantly more ductile than the base cements as evident by the decrease in Young's modulus (up to ~½ of base cement H and ½ of base TSRC using Zn salt/ BPA). Ductility is a critical property for cementitious materials used in geothermal wellbores since fracture propagation rates associated to thermal, mechanical, and/or chemical stresses can be significantly reduced. Mechanical property testing of these cement composite materials showed compressive strength above 1000 psi after 24 hours, as required for wellbore applications. Similarly, adhesion and re-adhesion to steel casing showed to be statistically similar or higher for polymer-cement composites as compared to base cements. Self-healing ability of these cement composites was studied using permeability analysis before and after healing a longitudinal fracture, most composites showed a consistently lower mean (post-

healing/pre-healing) permeability ratios than base (unmodified) cement H or TSRC cured for 5 days. To further test composite's thermal stability and capability for self-healing, the best-performing polymer-cement composite materials were exposed for 30-day at 300 °C. Permeability tests showed similar reduction in permeability post-healing as the 5-day cured samples. These results show that the composite materials are thermally stable and maintain their self-healing capability after 30 days exposure to elevated temperatures. These stability results were further confirmed by solid state ^{13}C NMR, TOC, and XRD. TOC and ^{13}C NMR which showed that the polymeric components were present in the cement composite supporting the stability of organic polymer at 300 °C after curing times of 10 and 30 days. XRD spectroscopy showed that most of the polymer-cement composites have identical mineralogy to their unmodified base cements.

In summary, these polymer-cement composites are more ductile, self-heal and have suitable mechanical properties and represent important alternatives to conventional wellbore cement for their application in geothermal and high-temperature oil wellbores.

5. ACKNOWLEDGEMENTS

Funding for this research was provided by the Department of Energy's Geothermal Technology Office. Pacific Northwest National Laboratory Computational resources were provided by PNNL Institutional Computing (PIC) and the National Energy Research Scientific Computing Center (NERSC), a DOE Office of Science User Facility supported by the Office of Science of the U.S. DOE is operated by Battelle for the U.S. DOE under contract DE-AC06-76RLO 1830.

6. REFERENCES

1. Hilloulin, B.; Van Tittelboom, K.; Gruyaert, E.; De Belie, N.; Loukili, A., Design of polymeric capsules for self-healing concrete. Cement and Concrete Composites 2015, 55, 298-307.
2. Walsh, S. D.; Du Frane, W. L.; Mason, H. E.; Carroll, S. A., Permeability of wellbore-cement fractures following degradation by carbonated brine. Rock Mech. Rock Eng. 2013, 46 (3), 455-464.
3. Childers, M. I.; Nguyen, M.-T.; Rod, K. A.; Koech, P. K.; Um, W.; Chun, J.; Glezakou, V.-A.; Linn, D.; Roosendaal, T. J.; Wietsma, T. W.; Huerta, N. J.; Kutchko, B. G.; Fernandez, C. A., Polymer-Cement Composites with Self-Healing Ability for Geothermal and Fossil Energy Applications. Chem. Mat. 2017, 29 (11), 4708-4718.
4. Van Tittelboom, K.; De Belie, N., Self-healing in cementitious materials—A review. Materials 2013, 6 (6), 2182-2217.
5. Wu, M.; Johannesson, B.; Geiker, M., A review: Self-healing in cementitious materials and engineered cementitious composite as a self-healing material. Construction and Building Materials 2012, 28 (1), 571-583.
6. Li, W.; Dong, B.; Yang, Z.; Xu, J.; Chen, Q.; Li, H.; Xing, F.; Jiang, Z., Recent Advances in Intrinsic Self-Healing Cementitious Materials. Advanced Materials 2018.
7. Huang, H. L.; Ye, G.; Qian, C. X.; Schlangen, E., Self-healing in cementitious materials: Materials, methods and service conditions. Materials & Design 2016, 92, 499-511.
8. Jiang, Z. W.; Li, W. T.; Yuan, Z. C., Influence of mineral additives and environmental conditions on the self-healing capabilities of cementitious materials. Cement & Concrete Composites 2015, 57, 116-127.
9. Van Tittelboom, K.; De Belie, N., Self-Healing in Cementitious Materials-A Review. Materials 2013, 6 (6), 2182-2217.
10. Reinhardt, H.; Jonkers, H.; Van Tittelboom, K.; Snoeck, D.; De Belie, N.; De Muynck, W.; Verstraete, W.; Wang, J.; Mechtcherine, V., Self-healing phenomena in cement-based materials : State-of-the-art report of rilem technical committee 221-shc: Self-healing phenomena in cement-based materials. In In RILEM State-of-the-art Reports 11, 2013; pp 65-117.
11. White, S. R.; Sottos, N.; Geubelle, P.; Moore, J.; Kessler, M. R.; Sriram, S.; Brown, E.; Viswanathan, S., Autonomic healing of polymer composites. Nature 2001, 409 (6822), 794.
12. Döhler, D.; Michael, P.; Binder, W. H., CuAAC-based click chemistry in self-healing polymers. Accounts of chemical research 2017, 50 (10), 2610-2620.
13. Krelani, V., Self-healing capacity of cementitious composites. 2015.
14. Tang, W. C.; Kardani, O.; Cui, H. Z., Robust evaluation of self-healing efficiency in cementitious materials - A review. Construction and Building Materials 2015, 81, 233-247.
15. Schlangen, E.; Sangadji, S., Addressing infrastructure durability and sustainability by self-healing mechanisms - recent advances in self healing concrete and asphalt. Procedia Engineering 2013, 54, 39-57.
16. Li, V. C.; Herbert, E., Robust self-healing concrete for sustainable infrastructure. Journal of Advanced Concrete Technology 2012, (10), 207-218.
17. Van Tittelboom, K.; De Belie, N.; De Muynck, W.; Verstraete, W., Use of bacteria to repair cracks in concrete. Cement and Concrete Research 2010, 40 (1), 157-166.
18. Jonkers, H. M., Bacteria-based self-healing concrete. Heron, 56 (1/2) 2011.
19. A) Nguyen, M.-T.; Wang, Z.; Rod, K. A.; Childers, M. I.; Fernandez, C.; Koech, P. K.; Bennett, W. D.; Rousseau, R.; Glezakou, V.-A., Atomic Origins of the Self-Healing Function in Cement–Polymer Composites. ACS Applied Materials & Interfaces 2018, 10 (3), 3011-3019. B) J. H. Lee, S. G. Kang, Y. Choe, S. G. Lee Composites Science and Technology 2016, 126, 9-16
20. Reddy, B. R.; Liang, F.; Fitzgerald, R. M.; Meadows, D., Self-repairing cement compositions and methods of using same. Google Patents: 2009.

21. Le Roy-Delage, S.; Martin-Beurel, M.; Dismuke, K.; Nelson, E., Self-adaptive cement systems. Google Patents: 2013.
22. Zhao, H.; Yu, H.; Yuan, Y.; Zhu, H., Blast mitigation effect of the foamed cement-base sacrificial cladding for tunnel structures. Construction and Building Materials 2015, 94, 710-718.
23. Snoeck, D.; Dewanckele, J.; Cnudde, V.; De Belie, N., X-ray computed microtomography to study autogenous healing of cementitious materials promoted by superabsorbent polymers. Cem. Concr. Compos. 2016, 65, 83-93.
24. Lee, H.; Wong, H.; Buenfeld, N., Self-sealing of cracks in concrete using superabsorbent polymers. Cement and Concrete Research 2016, 79, 194-208.
25. Canadell, J.; Goossens, H.; Klumperman, B., Self-healing materials based on disulfide links. Macromolecules 2011, 44 (8), 2536-2541.
26. Lafont, U.; Van Zeijl, H.; Van Der Zwaag, S., Influence of cross-linkers on the cohesive and adhesive self-healing ability of polysulfide-based thermosets. ACS applied materials & interfaces 2012, 4 (11), 6280-6288.
27. Pepels, M.; Filot, I.; Klumperman, B.; Goossens, H., Self-healing systems based on disulfide–thiol exchange reactions. Polymer Chemistry 2013, 4 (18), 4955-4965.
28. Rod, K. A.; Nguyen, M.-T.; Elbakhshwan, M.; Gillsc, S.; Kutchko, B.; Varga, T.; Mckinney, A. M.; Roosendaal, T. J.; Childers, M. I.; Zhaof, C.; Chen-Wiegartf, Y.-c. K.; Thiemeg, J.; Koech, P. K.; Um, W.; Chun, J.; Rousseau, R.; Glezakou, V.-A.; Fernandez, C. A., Insights into the physical and chemical properties of a cement-polymer composite developed for geothermal wellbore applications. Cement and Concrete Composites 2019, 97, 9.
29. Pyatina, T.; Sugama, T., Acid resistance of calcium aluminate cement-fly ash F blends. Advances in Cement Research 2016, 28 (7), 433-457.
30. Carpenter, R. B.; Brady, J. L.; Blount, C. G., EFFECTS OF TEMPERATURE AND CEMENT ADMIXES ON BOND STRENGTH. Journal of Petroleum Technology 1992, 44 (8), 880-&.
31. Zhao, X. F.; Guan, Z. C.; Xu, M. L.; Shi, Y. C.; Liao, H. L.; Sun, J., The Influence of Casing-Sand Adhesion on Cementing Bond Strength. Plos One 2015, 10 (6).
32. Miller, Q. R. S.; Kaszuba, J. P.; Schaef, H. T.; Bowden, M. E.; McGrail, B. P., Impacts of organic ligands on forsterite reactivity in supercritical CO2 fluids. Environ. Sci. Technol. 2015, 49 (7), 4724-4734.
33. Miller, Q. R. S.; Schaef, H. T.; Kaszuba, J. P.; Qiu, L.; Bowden, M. E.; McGrail, B. P., Tunable Manipulation of Mineral Carbonation Kinetics in Nanoscale Water Films via Citrate Additives. Environ. Sci. Technol. 2018, 52 (12), 7138-7148.
34. ASTM Standard Test Method for Splitting Tensile Strength of Intact Rock Core Specimens; West Conshohocken, PA, 2016.
35. Klute, A.; Dirksen, C., Hydraulic Conductivity and Diffusivity: Laboratory Methods. In Methods of Soil Analysis, Part 1 - Physical and Mineralogical Methods, Klute, A., Ed. American Society of Agronomy, Inc, Soil Science Society of America, Inc,: Madison, WI, 1986; pp 687-734.
36. ASTM Standard Test Methods for Measurement of Hydraulic Conductivity of Saturated Porous Materials Using a Flexible Wall Permeameter; West Conshohocken, PA, 2010.
37. Bear, J., Dynamics of Fluids in Porous Media. American Elsevier Publishing Company, Inc.: 1972.
38. Carey, J. W.; Svec, R.; Grigg, R.; Zhang, J.; Crow, W., Experimental investigation of wellbore integrity and CO2-brine flow along the casing-cement microannulus. International Journal of Greenhouse Gas Control 2010, 4 (2), 272-282.
39. Assaad, J. J., Development and use of polymer-modified cement for adhesive and repair applications. Construction and Building Materials 2018, 163, 139-148.
40. Rod, K.A., et al., *Polymer-cement composites with adhesion and re-adhesion (healing) to casing capability for geothermal wellbore applications.* Cement and Concrete Research - under review, 2019
41. Noushini, A.; Aslani, F.; Castel, A.; Gilbert, R. I.; Uy, B.; Foster, S., Compressive stress-strain model for low-calcium fly ash-based geopolymer and heat-cured Portland cement concrete. Cement and Concrete Composites 2016, 73, 136-146.
42. Şahmaran, M.; Keskin, S. B.; Ozerkan, G.; Yaman, I. O., Self-healing of mechanically-loaded self-consolidating concretes with high volumes of fly ash. Cement and Concrete Composites 2008, 30 (10), 872-879.